Applied Catalysis B: Environmental 227 (2018) 54–60

Contents lists available at ScienceDirect

Applied Catalysis B: Environmental

journal homepage: www.elsevier.com/locate/apcatb

Assembly of highly efficient photocatalytic CO_2 conversion systems with ultrathin two-dimensional metal–organic framework nanosheets

Lu Ye[a], Yan Gao[a,*], Shuyan Cao[a], Hu Chen[a], Yanan Yao[a], Jungang Hou[a], Licheng Sun[a,b]

[a] State Key Laboratory of Fine Chemicals, DUT-KTH Joint Education and Research Centre on Molecular Devices, Dalian University of Technology (DUT), Dalian 116024, China

[b] Department of Chemistry, KTH Royal Institute of Technology, Stockholm 10044, Sweden

ARTICLE INFO

Keywords:
CO_2 reduction
Photocatalysis
Metal–organic frameworks
Nanosheets
Zn porphyrin

ABSTRACT

An ultrathin two-dimensional Zn porphyrin-based metal–organic framework (Zn-MOF nanosheets) is developed and used for the first time in photoreduction of CO_2 to CO. Consequently, two novelty noble-metal-free hybrid photocatalytic systems are established and displayed outstanding photocatalytic activity and selectivity for CO evolution under mild photocatalytic reaction conditions. The insight revealed Zn-MOF nanosheets as photosensitizer displays a better charge transport ability and longer lifetime of the photogenerated electron-hole pairs than the Zn-MOF bulk, which are confirmed by photoelectrochemical impedance and photoluminescence (PL) measurements. These studies show that the development of noble-metal-free photocatalytic systems and various MOF-based materials for photocatalytic applications are promising.

1. Introduction

Global climate change and the increasing energy demand have had a serious impact on human society [1–3]. Therefore, mimicking photosynthesis, which converts of CO_2 into fuels and chemical feedstocks using solar energy, would be of great benefit. The photoreduction of CO_2 is extremely difficult because CO_2 is a stable linear molecule, so a large energy is required to change its geometry from linear to bent [4]. Herein, we report on the development of highly efficient and selective photocatalytic systems for the photochemical reduction of CO_2.

So far, photocatalytic systems containing a metal complex as co-catalyst and a dye molecule as photosensitizer have been studied extensively owing to their high selectivity for products [5–10]. However, most of the dye molecules in the system contain a noble metal, such as Ir and Ru [6–9], which hinders their practical applications. In addition, these photocatalytic systems are unstable owing to the photodegradation of the dye molecules under light irradiation [5,7,10]. To solve these problems, the use of stable semiconductors to replace the dye molecules is a promising approach. Ishitani and co-workers have designed a hybrid photocatalytic system containing an homogeneous metal complex and a heterogeneous semiconductor [11–14]. This system was more stable and efficient than the previously reported homogeneous photocatalytic systems; [11–13] however, the efficiency of this system was drastically reduced when a noble-metal-free complex was used as the catalyst instead of the Ru and Re complexes [14]. Therefore, an ideal solution would be to incorporate a highly efficient noble-metal-free co-catalyst together with a photosensitizer that possesses a high light absorption ability and photostability.

Metal – organic frameworks (MOFs), as a new class of hybrid materials that consist of an organic linker and secondary building units, have been extensively researched for decades and have been demonstrated to possess promising applications in various fields [15–18]. Recently, MOFs have been developed as photocatalysts and electrocatalysts to reduce CO_2 to fuels owing to their assistance in CO_2 capture and activation [19–23]. Porphyrin-based MOFs, considered as semiconductors owing to their high light absorption ability, have also been studied for the photochemical reduction of CO_2 [24]. However, the efficiency of bulk porphyrin-based MOFs is too low, mainly as a result of the fast charge recombination of the photogenerated electron-hole pairs [25]. Compared with bulk MOFs, 2D MOF nanosheets possess higher photocatalytic efficiency, because of the synergistic effect of the increased surface area and CO_2 adsorption, enhanced electron-transport properties, and prolonged lifetime of the photogenerated electron-hole pairs. However, without co-catalyst, the efficiency of porphyrin-based MOFs is very low for the photocatalytic CO_2 reduction [26]. Therefore, an attractive approach is to develop a new photocatalytic system which contains a 2D porphyrin-based MOF as photosensitizer and a noble-metal-free complex or ZIF as co-catalysts.

Herein, we report a simple synthetic method for a uniformed ultrathin 2D Zn porphyrin (5,10,15,20-tetrakis(4-carboxyphenyl) porphyrin;

* Corresponding author.
E-mail address: dr.gaoyan@dlut.edu.cn (Y. Gao).

https://doi.org/10.1016/j.apcatb.2018.01.028
Received 2 November 2017; Received in revised form 8 January 2018; Accepted 14 January 2018

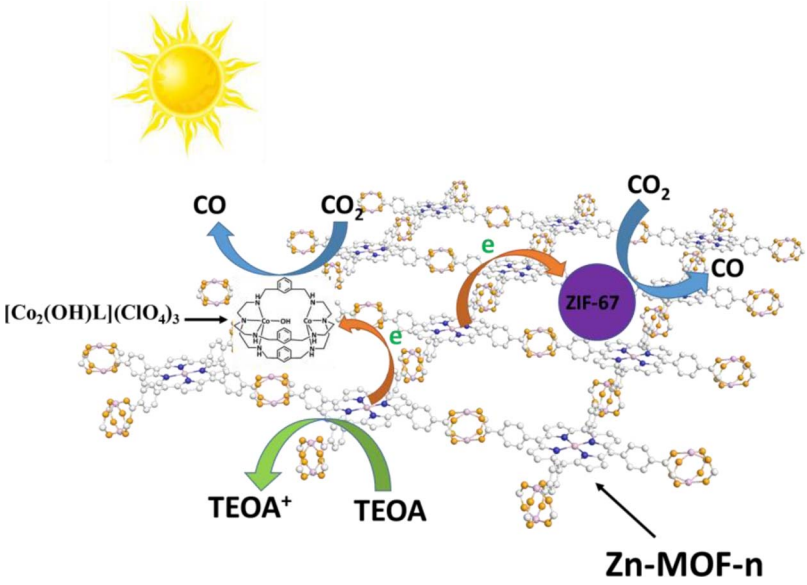

Scheme 1. A MOF/complex or MOF/ZIF system for CO_2 photoreduction with Zn-MOF nanosheets as the photosensitizer.

TCPP)-based MOF (denoted as Zn-MOF nanosheets) with a thickness of approximately 4.7 nm. Consequently, a Zn-MOF nanosheets or Zn-MOF bulk was applied as the photosensitizer with a dinuclear cobalt complex $[Co_2(OH)L](ClO_4)_3$(L = $N[(CH_2)_2NHCH_2(m\text{-}C_6H_4)CH_2NH(CH_2)]_3N$) or ZIF-67 as co-catalyst in a MOF/complex or MOF/ZIF system for CO_2 photoreduction (Scheme 1). Compared with the Zn-MOF bulk, the Zn-MOF nanosheets displayed a higher photocatalytic activity and selectivity for CO evolution in these systems mainly arising from their better CO_2 adsorption capacity and charge transport ability, as well as the longer lifetime of the photogenerated electron-hole pairs.

2. Experimental

2.1. Synthesis of Zn-MOF nanosheets

$Zn(NO_3)_2{\cdot}6H_2O$ (2.25 mg, 0.0075 mmol), PVP (10.0 mg) and pyrazine (0.4 mg, 0.005 mmol) were dissolved in a solution of DEF/DMF/EtOH (24 mL, v:v:v = 2:1:1). Then TCPP (2.0 mg, 0.0025 mmol) dissolved in 8 mL DMF/EtOH (v:v = 2:1) was added dropwise. The solution was stirred under sonication for 30 min and then heated to 80 °C for 16 h. The reaction mixture was then cooled naturally, the desired purple nanosheets were collected by high speed centrifugalization and washed with DMF and EtOH for several times.

2.2. Characterization

X-ray diffraction (XRD) measurements were carried out by a Rigaku D/MAX2400 diffractometer for the co-planar (out-of-plane, OP) measurement in θ-θ geometry. The XRD data were acquired over a 2θ range of 5–23°. The optical properties were measured by a UV–vis absorption spectroscopy (Agilent 8453). The photoluminescence spectra were measured with a fluorescence spectrophotometer. X-ray photoelectron spectroscopy (XPS) experiments were performed in an ultra-high vacuum system (base pressure 2×10^{-10} mbar) equipped with a non-monochromatic Al Kα X-ray source and a hemispherical energy analyzer (VG-Scienta R4000). The instrumental resolution was less than 500 meV. Atomic force microscopy (AFM) was employed by DI Innova Multimode SPM system. The morphologies and sizes of the Zn-MOF nanosheets and the Zn-MOF bulk were imaged by scanning electron microscopy (SEM) (NOVA NanoSEM 450) and transmission electron microscopy (TEM) (FEI Tecnai G2F20 S-TWIN). Gas adsorption measurement was performed through the ASAP 2020 system. The specific surface area of the photocatalysts was calculated by the Brunauer-Emmett-Teller (BET) method. Thermogravimetric analysis (TGA) was performed in air with a heating rate of 10 °C per minute. Photoelectrochemical properties were measured in a three-electrode system with 0.5 M Na_2SO_4 solution as electrolyte. The Zn-MOF nanosheets or the Zn-MOF bulk was deposited on a FTO conducting glass as working electrode with a working area of 1 cm^2. The suspension for the deposition was 0.2 mL ethanol containing 0.2 mg of the samples. Pt electrode and Ag/AgCl electrode (saturated KCl solution) were used as the counter and reference electrodes.

2.3. Photocatalytic reaction

The photocatalytic reaction was performed in a solution (6 mL, MeCN/MeOH/TEOA = 4:1:1) containing Zn-MOF nanosheets or Zn-MOF bulk (10 mg) as photosensitizer, $[Co_2(OH)L](ClO_4)_3$ or ZIF-67 as co-catalyst and TEOA as electron donor. The photocatalytic system was purged with CO_2 (99.999%) for 30 min and then irradiated for 6 h under a Xe lamp (120 mW cm^{-2}) with a 420 nm cutoff filter. The collected H_2 was analyzed by a gas chromatograph (GC, Techcomp 7890) equipped with thermal conductivity and the CO was test using a GC (Techcomp 7900) equipped with flame ionization detectors. The photocatalytic system with ZIF-67 as co-catalyst was constructed and operated under similar conditions with using $[Co_2(OH)L](ClO_4)_3$ as co-catalyst. Multiple photocatalysis experiments were run at each condition and the average data was calculated.

2.4. Absorption/emission measurements

UV–vis spectroscopy was carried out by a Agilent 8453 diode array spectrophotometer and emission spectroscopy was carried out by a Fluoro Max-4P fluorescence spectrometer, at room temperature using 1 cm quartz cell (light path length = 1 cm).

The quenching rate was determined by the Stern-Volmer equation:

$$\frac{I_0}{I} = 1 + k_q \tau_0 [Q]$$

Where I_0 and I are the fluorescence intensity of the Zn-MOF nanosheets or the Zn-MOF bulk in the absence and presence of the quencher Q. k_q is the quenching rate constant. τ_0 is the fluorescence lifetime of the excited state in the absence of the quencher Q, which was determined to be 0.51 ns (Zn-MOF nanosheets) and 0.33 ns (Zn-MOF bulk) in MeCN/MeOH (v/v, 4:1) solution based on the time-resolved PL spectra. [Q] is the concentration of the quencher Q. In the tests, the concentration of

Zn-MOF nanosheets or Zn-MOF bulk was a constant of 10 μg L^{-1}. The emission wavelength was 651 nm with the excitation wavelength fixed at 432 nm.

2.5. Quantum efficiency (QE) measurement

Same to the photocatalytic reaction, 6 mL mixture solution (MeCN/MeOH/TEOA = 4:1:1) containing Zn-MOF nanosheets or Zn-MOF bulk (10 mg) and $[Co_2(OH)L](ClO_4)_3$ (10 nmol) in a Shrek bottle was irradiated under the monochromic light of 435 nm wavelength with a cut-off filter. The entering light was supposed to be fully absorbed by the photosensitizer according to the Beer-Lambert law. The light intensity was determined to be 12 mW cm^{-2} with a CEAULIGHT CEL-NP 2000 laser power meter right. The QE with ZIF-67 as co-catalyst was constructed and operated under similar conditions with using $[Co_2(OH)L](ClO_4)_3$ as co-catalyst. The calculation of the apparent quantum yield was according to equation:

$$\Phi_{CO} = \frac{2n_{co}Nhc}{P\lambda t} \quad (1)$$

Where n_{co} is the amount of CO. N is Avogadro constant. h is Planck constant. c is velocity of light. P is light intensity. λ is wavelength of light. t is the time of photocatalytic reaction.

3. Results and discussion

The Zn-MOF bulk was synthesized by a simple method that has been reported in the literature [27,28]. The surfactant-assisted method was used to prepare the uniformed 2D Zn-TCPP nanosheets. Briefly, zinc nitrate, TCPP, and pyrazine were added to a solution of DEF/DMF/EtOH (v:v:v = 2:1:1), then a solution of DEF/DMF/EtOH containing surfactant polyvinylpyrrolidone (PVP) was added. The PVP can selectively attach to the specific facets of MOFs during the preparation of Zn-MOF nanosheets. In this kind of 2D Zn-MOF nanosheet, one TCPP is conjecturally linked by four Zn. Under the reaction conditions, the TCPP could be metallized by Zn^{2+} ions.

The XRD patterns of Zn-MOFs were performed, as shown in Fig. S1. The four characteristic peaks, located at 5.3°, 7.5°, 8.8°, and 18.0°, were indexed to the (100), (110), (002), and (004) diffraction planes of Zn-MOF nanosheets and Zn-MOF bulk [29], indicating their same crystal structure. The scanning electron microscopy (SEM) images of the Zn-MOFs showed the distinct appearances of the bulk and nanosheets (Fig. S2). Transmission electron microscopy (TEM) (Fig. 1a) further confirmed the ultra-thin sheet structure of Zn-MOF nanosheets. Atomic force microscopy (AFM) images (Fig. 1c–d) showed that the average thickness of Zn-MOF nanosheets was approximately 4.7 nm, so the prepared Zn-MOF nanosheets were determined to be composed of 5 layers because the theoretical inter-layer distance is 0.93 [27]. Energy dispersive X-ray elemental (EDX) mappings (Fig. 1b) obtained by TEM confirm the coexistence of Zn, C, O, and N, and the Zn element was uniformly distributed on the MOF nanosheets. The X-ray photoelectron spectroscopy (XPS) peak (Fig. 1Figs. 1e and S2) of the Zn-MOF nanosheets indicated the presence of Zn, C, O, and N, in accordance with the results of the EDX mappings. Fig. 1e shows the high resolution XPS spectra of Zn 2p. The two signals at 1044.9 and 1022.0 eV, which correspond to Zn $2P_{1/2}$ and Zn $2P_{3/2}$, were assigned to the binding energy of Zn^{2+} [30]. The specific surface areas of Zn-MOF bulk and Zn-MOF nanosheets were investigated by nitrogen adsorption experiments, and showed similar approximate type I Langmuir isotherms (Fig. S4) [27,28].

The Brunauer-Emmett-Teller (BET) surface area of Zn-MOF nanosheets was 445 $m^2 g^{-1}$, which is larger than that of the Zn-MOF bulk (295 $m^2 g^{-1}$). The stability of the Zn-MOF nanosheets was examined by thermogravimetric (TG) analysis (Fig. S5). The weight loss from 25 to 200 °C corresponded to the loss of solvent molecules within the MOF channels and pores and the weight loss after 400 °C corresponded to the decomposition of the TCPP ligand. This result shows the high thermal stability of the Zn-MOFs up to 400 °C. To study the optical property of the Zn-MOFs, the UV–vis absorption spectra were measured (Fig. 1f). The absorption spectrum of the TCPP ligand consisted of a Soret band at 417 nm and four Q-bands at 513, 548, 592, and 644 nm, which are in good agreement with the literature [28]. The Zn-MOF nanosheets displayed a red-shifted Soret band at 434 nm (compared to 417 nm for TCPP) and only two predominant Q-bands at 562 and 599 nm instead of four Q bands because of the higher symmetry of the metalized compound, which indicate the successful metalation of the porphyrin rings by Zn^{2+} ions [28].

The activity of a MOF/complex hybrid system on the photocatalytic reduction of CO_2 was performed in a MeCN/MeOH/TEOA solvent (MeOH as the proton donor and TEOA as sacrificial agent) by visible-light irradiation under mild reaction conditions, with $[Co_2(OH)L](ClO_4)_3$ as co-catalyst, and the Zn-MOF nanosheets or Zn-MOF bulk as photosensitizer. With Zn-MOF bulk as photosensitizer, the turnover numbers (TONs) of CO and H_2 obtained within 6 h irradiation were calculated to be 26.2 and 12.4, respectively, while the TONs of CO and H_2 increased to 68.7 and 15.6 when using Zn-MOF nanosheets as photosensitizer (Fig. 2a). The selectivity for CO evolution (Table S1) with Zn-MOF nanosheets (81.5%) was also higher than that with Zn-MOF bulk (67.9%).

Control experiments (Table 1) were conducted to study the influences of the components in this photocatalytic CO_2 reduction system. When the Zn-MOF nanosheets were not included in the system, no products were detected, which indicated that the Zn-MOF nanosheets as the photosensitizer undergoes photoexcitation upon visible-light illumination for the photoreduction of CO_2. Additionally, only trace amounts of H_2 product were obtained when the system excluded the co-catalyst $[Co_2(OH)L](ClO_4)_3$, which indicated that the co-catalyst is also necessary in the photocatalytic system. This revealed that other components (CO_2, electron donor, and light source) were also necessary for the photoreduction of CO_2 to CO. When $^{13}CO_2$ was used to replace $^{12}CO_2$ under the same photoreduction conditions, the detected ^{13}CO firmly proved that the produced CO stemmed from the photoreduction of CO_2 and not from other sources (Fig. S6).

The photocatalytic activity of the MOF/ZIF system was also investigated under the same conditions by using ZIF-67 as co-catalyst. When using Zn-MOF nanosheets as photosensitizer, Fig. 2b shows that a higher photocatalytic activity and selectivity for CO (TON_{CO} = 117.8, TON_{H2} = 11.6, and $selectivity_{CO}$ = 91.0%) than that using Zn-MOF bulk as photosensitizer (TON_{CO} = 63.6, TON_{H2} = 7.5, and $selectivity_{CO}$ = 89.5%) was achieved. Control experiments were also conducted (Table S1), and showed the necessity for Zn-MOF nanosheets as the photosensitizer owing to the low light absorption ability of ZIF-67.[13] The photocatalytic efficiency of these presently designed systems is higher than most MOF-based and semiconductors/complex hybrid photocatalytic systems reported to date under mild photocatalytic reaction conditions (Table S4) [32–40].

To study the stability of Zn-MOF nanosheets in the MOF/complex and MOF/ZIF photocatalytic systems, the experiments were conducted for three cycles. After each cycle, the system was refilled with CO_2 for 30 min until no products were found remaining, while keeping co-catalyst and other components as constant. After 3 cycles, the CO production decreased by 24% for the MOF/complex system (Fig. S8) and 19% for the MOF/ZIF system (Fig. S9). These results show that Zn-MOF nanosheets are more stable than molecular dye photosensitizers for the photoreduction of CO_2 reaction under visible light (420 nm < λ < 800 nm) [5–10]. To gain a better understanding of the stability of the Zn-MOF nanosheets, XRD (Fig. S12) and UV–vis absorption spectra (Fig. S13) were used to characterize the Zn-MOF nanosheets after photocatalysis. No significant differences between the fresh sample and tested samples were observed, thus suggesting the stability of the Zn-MOF nanosheets in the photocatalytic CO_2 reduction system.

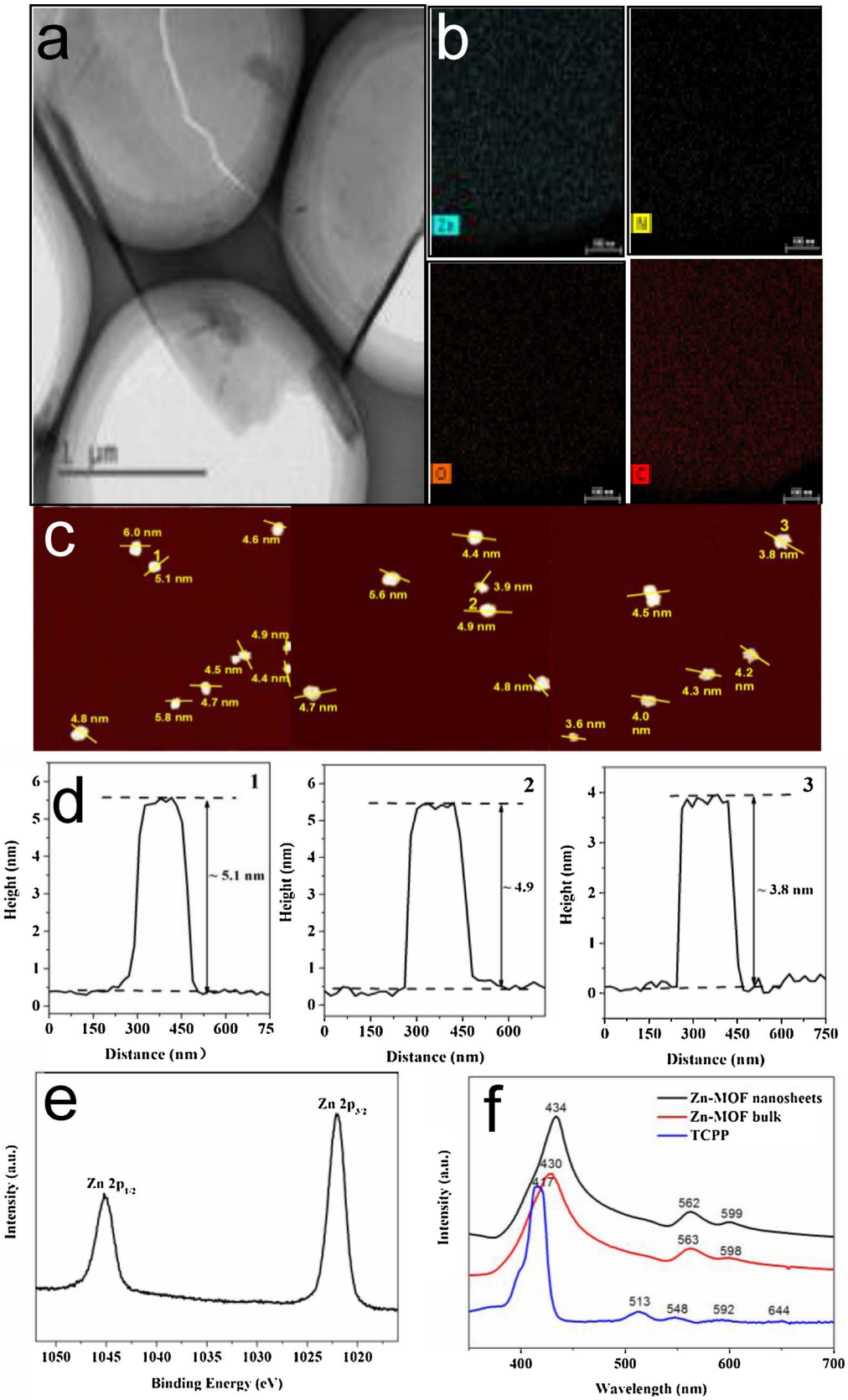

Fig. 1. Characterizations for the Zn-MOF nanosheets. (a-b) TEM image and the corresponding EDX mapping images, (c-d) AFM images, (e) XPS spectrum of Zn, (f) UV–vis absorption spectra.

The CO_2 adsorption capacity over Zn-MOF nanosheets was measured to be 103.8 $cm^3 g^{-1}$ (Fig. 3a), which is higher than that of Zn-MOF bulk (59.9 $cm^3 g^{-1}$). Although the photoreduction of CO_2 does not occur on the surface of the Zn-MOF nanosheets, the higher adsorption capacity of CO_2 on the Zn-MOF nanosheets can improve the photocatalytic efficiency in the MOF/complex hybrid system. During the photocatalysis process, a $Co_2[(OH)L](ClO_4)_3$ must be infinitely close to the surface of the Zn-MOF nanosheets, thus the high adsorption

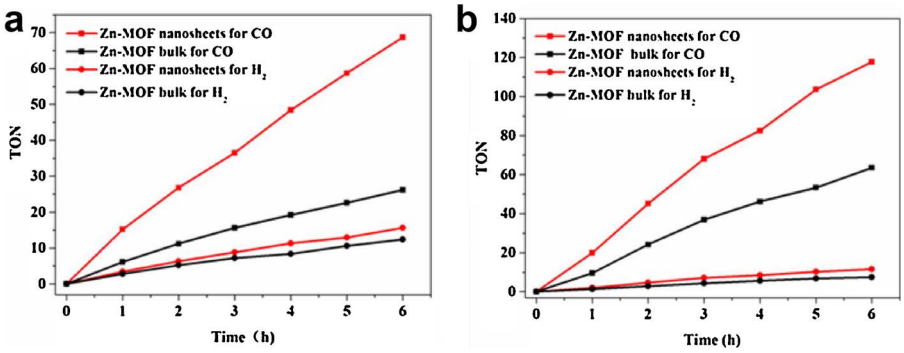

Fig. 2. Evolution of the CO_2 photocatalytic reduction products under Xe lamp irradiation (120 mW cm^{-2}, 420 nm < λ < 800 nm) for 6 h. (a) Zn-MOF nanosheets or Zn-MOF bulk as photosensitizer and $[Co_2(OH)L](ClO_4)_3$ as co-catalyst, (b) Zn-MOF nanosheets or Zn-MOF bulk as photosensitizer and ZIF-67 as co-catalyst.

Table 1
Photocatalysis with Zn-MOF nanosheets as photosensitizer and $[Co_2(OH)L](ClO_4)_3$ as co-catalyst.

entry	CO (nmol)	TON_{CO}	H_2 (nmol)	TON_{H2}	$Selectivity_{CO}$[b](%)
1[a]	687	68.7	156	15.6	81.5
2[c]	262	26.2	124	12.4	67.9
3[d]	n.d.[e]	n.d.	113	/	0
4[f]	n.d.	n.d.	67	/	0
5[g]	n.d.	n.d.	n.d.	n.d.	/
6[h]	n.d.	n.d.	n.d.	n.d.	/
7[i]	n.d.	n.d.	n.d.	n.d.	/

[a] Reaction conditions: $[Co_2(OH)L](ClO_4)_3$ (10 nmol), Zn-MOF nanosheets (10 mg), solution (6 mL, MeCN/MeOH/TEOA = 4:1:1), light source (Xe lamp: 120 mW cm^{-2}) with a 420 nm cutoff filter, CO_2 (99.999%), reaction time (6 h).
[b] $Selectivity_{CO} = n_{CO}/(n_{CO}+n_{H2}) \times 100\%$.
[c] Substituting Bulk Zn-MOF for Zn-MOF nanosheet.
[d] Substituting Ar for CO_2.
[e] Not detectable.
[f] Without co-catalyst ($[Co_2(OH)L](ClO_4)_3$).
[g] Without electron donor (TEOA).
[h] Without photosensitizer.
[i] In the dark.

capacity makes the catalyst trap a CO_2 molecule easily from the surface of Zn-MOF nanosheets to perform photoreduction of CO_2. However, in the MOF/ZIF system, both the Zn-MOF nanosheets and the ZIF-67 possess an excellent adsorption capacity of CO_2, which results in a higher photocatalytic efficiency for CO_2 reduction [31].

Moving from the heterogeneous photocatalytic systems to photoelectrochemical devices, photoelectrodes were assembled to investigate the photocurrent generation behaviors of the Zn-MOFs under visible-light irradiation (Fig. 3b). With application of a −0.2 V NHE external bias, the photocurrent density of the Zn-MOF nanosheets photoelectrode was obviously higher than that of Zn-MOF bulk photoelectrode, which indicated a more efficient separation and longer lifetime of photogenerated charge carriers with the Zn-MOF nanosheets [32]. The electrochemical impedance spectra of the Zn-MOFs were further employed to detect the charge-transport behavior (Fig. 3c). The charge-transfer resistance of the Zn-MOF nanosheets electrode was obviously lower than that of the Zn-MOF bulk electrode, which corresponded to its higher speed of charge separation of the electron-hole pairs and the interfacial charge transfer [32], and agreed well with their photocatalytic performances as discussed above. The steady-state PL spectra illustrated that the emission intensity of the Zn-MOF nanosheets was lower than that of the Zn-MOF bulk, indicating the greatly suppressed

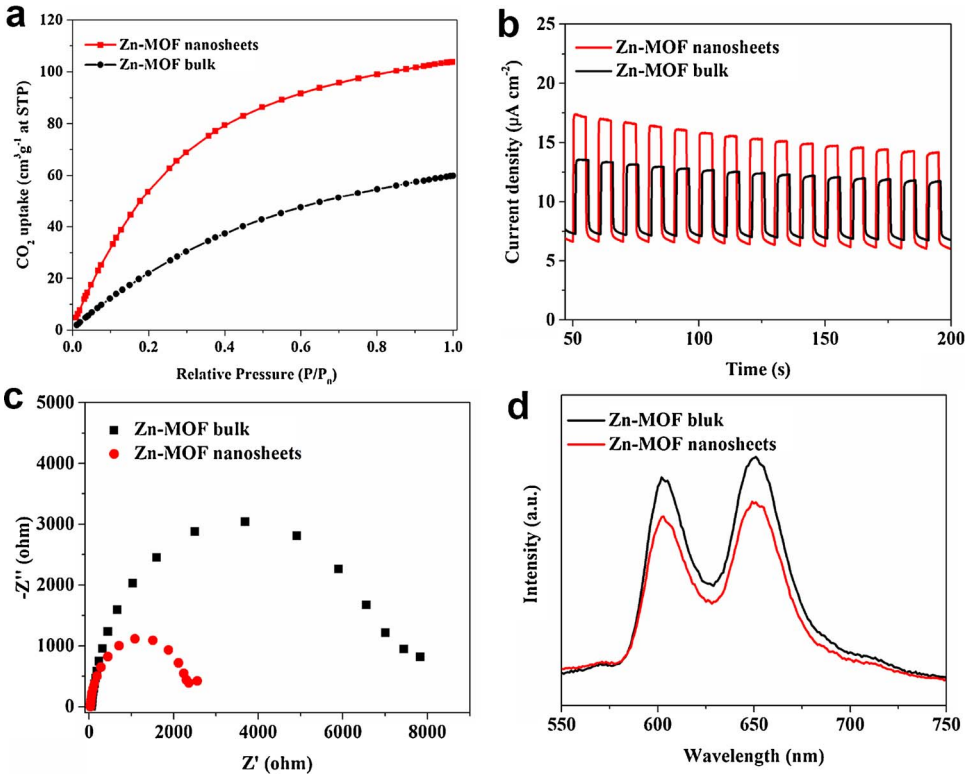

Fig. 3. Comparisons between Zn-MOF nanosheets and Zn-MOF bulk. (a) CO_2 adsorption capacities, (b) photocurrent–time profiles, Zn-MOF nanosheets on FTO as working electrode, Pt as counter electrode, Ag/AgCl as reference electrode in 0.2 M Na_2SO_4 aqueous solution, (c) electrochemical impedance spectra, and (d) PL spectra.

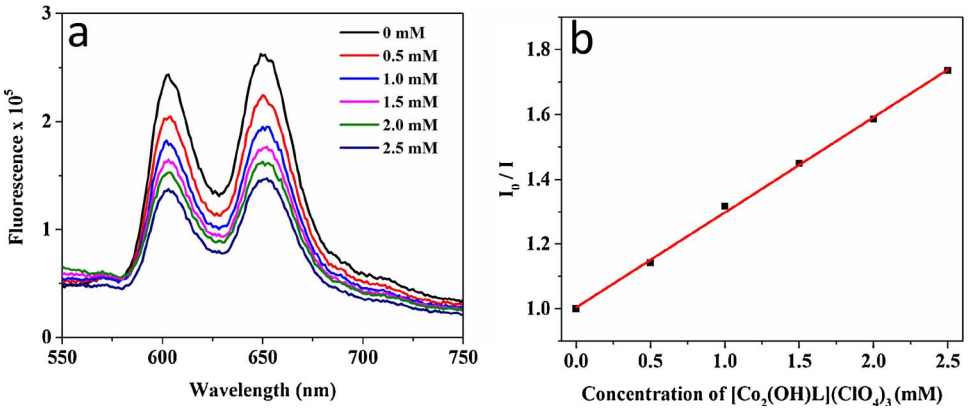

Fig. 4. (a) Fluorescence spectra of Zn-MOF nanosheets (10 μg L^{-1}) in MeCN/MeOH (v/v = 4:1) solution containing $[Co_2(OH)L](ClO_4)_3$ (various concentrations). (b) Stern-Volmer plot for fluorescence intensity quenching of Zn-MOF nanosheets (10 μg L^{-1}) by co-catalyst $[Co_2(OH)L](ClO_4)_3$.

radiative electron-hole recombination [34]. All these results indicate that Zn-MOF nanosheets possess a better charge transport ability that is beneficial for improving the efficiency of photocatalytic CO_2 reduction.

To understand more about the mechanism of photoinduced electron transfer in the MOF/complex hybrid photocatalytic system, the quenching of the excited state of Zn-MOFs by $Co_2[(OH)L](ClO_4)_3$ was measured from the steady-state photoluminescence (PL) spectra with an excitation wavelength of 432 nm (Fig. 4Figs. 4 and S15). Both the Zn-MOFs followed a good Stern-Volmer behavior in the MOF/complex hybrid system [41]. The quenching rate constant of the Zn-MOF nanosheets was $5.76 \times 10^{12}\ M^{-1}\ s^{-1}$ (k_{q1}), which is higher than that of the Zn-MOF bulk ($1.77 \times 10^{12}\ M^{-1}\ s^{-1}$, k_{q2}). A higher quenching rate constant indicates a faster electron transfer from the Zn-MOF to the co-catalyst as well as a slower recombination of the photogenerated electron-hole pairs, and thereby improves the photocatalytic CO_2 efficiency.

Additionally, quenching of the excited state of Zn-MOF nanosheets by TEOA was also studied (Fig. S16). A good Stern-Volmer behavior was observed and the quenching rate constant was $2.89 \times 10^{12}\ M^{-1}\ s^{-1}$ (k_{q3}). Considering the concentration of TEOA was 7.5×10^5 times higher than that of $[Co_2[(OH)L](ClO_4)_3$, although k_{q3} was approximately half of k_{q1}, the result still suggests that direct reductive quenching of Zn-MOF nanosheets by TEOA is more favorable than the oxidative quenching of Zn-MOF nanosheets by $[Co_2(OH)L](ClO_4)_3$ in the MOF/complex hybrid photocatalytic system.

Based on our studies and Lu's recent work [42], we propose a reasonable photoredox cycle for the reduction of CO_2 to CO (Scheme 2). The photocatalytic CO_2 reduction starts from the excitation of ZnTCPP (a unit of Zn-MOF nanosheets) by visible-light irradiation to form [ZnTCPP]*, which is then reductively quenched by TEOA to generate $[ZnTCPP]^-$. $[Co_2(OH)L]^{3+}$ containing $Co_2^{II,II}$ fixes CO_2 to generate a carbonate-bridged complex **a**, which undergoes proton-coupled electron transfer (PCET) reduction to afford intermediate **b** ($Co_2^{II,III}$) by $[ZnTCPP]^-$. According to the literature [27], the reduction potential of $[ZnTCPP]^-$ is more negative than that of $Co_2^{II,II}/Co_2^{II,I}$ (−1.00 V), which makes the reduction of **a** into a $Co_2^{II,I}$ species by $[ZnTCPP]^-$ thermodynamically feasible, and then to form **b** by protoncoupling. Subsequently, **b** undergoes another PCET reduction by $[ZnTCPP]^-$ to form **c**, where the reduction potential for $Co_2^{II,III}/Co_2^{II,II}$ is −0.85 V vs. NHE. This large thermodynamic advantage makes the charge quickly transferred from $[ZnTCPP]^-$ to **b** to form intermediate **c**. Finally, intermediate **c** liberates a CO and completes the CO_2 photoreduction cycle.

In summary, a MOF/complex or MOF/ZIF system, which contains Zn-MOF as semiconductor photosensitizer and $[Co_2(OH)L](ClO_4)_3$ or ZIF-67 as co-catalyst, has been developed for the photochemical reduction of CO_2 with high efficiency, selectivity, and stability. To the best of our knowledge, this kind of MOF/ZIF system has been developed for the first time and the Zn-MOF nanosheets have not yet been applied in CO_2 photoreduction. Compared with Zn-MOF bulk, these photocatalytic systems exhibit an enhanced photocatalytic efficiency and selectivity for CO evolution when using Zn-MOF nanosheets as photosensitizer. The photoelectrochemical impedance and PL studies indicated that the photocatalytic enhancement mainly arises from the better charge transport ability, and the more efficient separation and longer lifetime of photogenerated charge carriers with the Zn-MOF nanosheets. This work provides a new route to design efficient and stable noble-metal-free photocatalytic systems for the photochemical

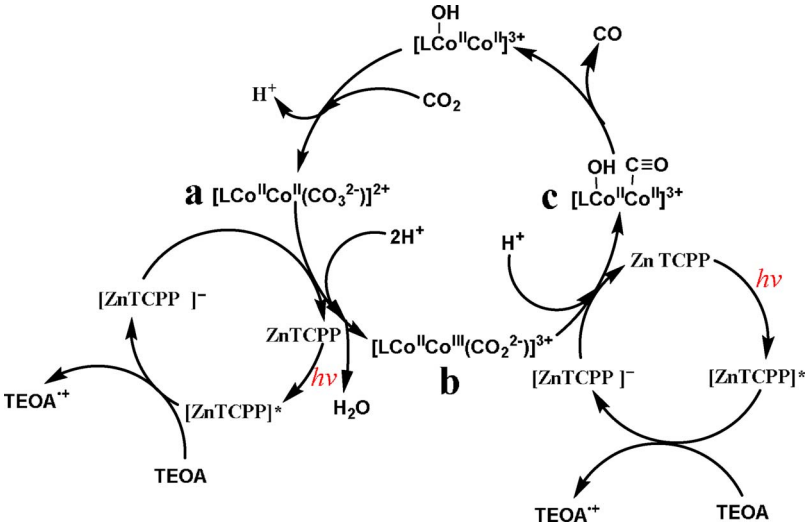

Scheme 2. Proposed photocatalytic mechanism of Zn-MOF nanosheets with $[Co_2[(OH)L](ClO_4)_3$ for the visible-light driven photocatalytic CO_2 reduction reaction.

reduction of CO_2, as well as to provide opportunities to develop various 2D MOF-based materials for photocatalytic applications.

Acknowledgements

This work was supported by the National Natural Science Foundation of China (21573033), the National Basic ResearchProgram of China (973 program, 2014CB239402), the Swedish Energy Agency and the K & A Wallenberg Foundation.

Appendix A. Supplementary data

Supplementary data associated with this article can be found, in the online version, at https://doi.org/10.1016/j.apcatb.2018.01.028.

References

[1] X.X. Chang, T. Wang, J.L. Gong, Energy Environ. Sci. 9 (2016) 2177–2196.
[2] W. Kim, B.A. McClure, E. Edri, H. Frei, Chem. Soc. Rev. 45 (2016) 3221–3243.
[3] Y.P. Yuan, L.W. Ruan, J. Barber, S.C.J. Loo, C. Xue, Energy Environ. Sci. 7 (2014) 3934–3951.
[4] J. Schneider, H.F. Jia, J.T. Muckerman, E. Fujita, Chem. Soc. Rev. 41 (2012) 2036–2051.
[5] Z.G. Guo, S.W. Cheng, C. Cometto, E.A. Mallart, S.M. Ng, C. Ko, G.J. Liu, L.J. Chen, M. Robert, T.C. Lau, J. Am. Chem. Soc. 138 (2016) 9413–9416.
[6] Y. Kou, Y. Nabetani, D. Masui, T. Shimada, S. Takagi, H. Tachibana, H. Inoue, J. Am. Chem. Soc. 136 (2014) 6021–6030.
[7] Y. Tamaki, K. Koike, O. Ishitani, Chem. Sci. 6 (2015) 7213–7221.
[8] K. Garg, Y. Matsubara, M.Z. Ertem, A.L. Andralojc, S. Sato, D.J. Szalda, J.T. Muckerman, E. Fujita, Angew. Chem. Int. Ed. 54 (2015) 14128–14132.
[9] S. Sato, T. Morikawa, T. Kajino, O. Ishitani, Angew. Chem. Int. Ed. 52 (2013) 988–992.
[10] D. Hong, Y. Tsukakoshi, H. Kotani, T. Ishizuka, T. Kojima, J. Am. Chem. Soc. 139 (2017) 6538–6541.
[11] K. Maeda, K. Sekizawa, O. Ishitani, Chem. Commun. 49 (2013) 10127–10129.
[12] K. Maeda, R. Kuriki, M.W. Zhang, X.C. Wang, O. Ishitani, J. Mater. Chem. A 2 (2014) 15146–15151.
[13] R. Kuriki, O. Ishitani, K. Maeda, ACS Appl. Mater. Interfaces 8 (2016) 6011–6018.
[14] M.F. Kuehnel, K.L. Orchard, K.E. Dalle, E. Reisner, J. Am. Chem. Soc. 139 (2017) 7217–7223.
[15] F.F. Cao, M.T. Zhao, Y.F. Yu, B. Chen, Y. Huang, J. Yang, X.H. Cao, Q.P. Lu, X. Zhang, Z.C. Zhang, C.L. Tan, H. Zhang, J. Am. Chem. Soc. 138 (2016) 6924–6927.
[16] T.H. Chang, Chung-Wei Kung, Hsin-Wei Chen, Tzu-Yen Huang, Sheng-Yuan Kao, H.C. Lu, M.H. Lee, K.M. Boopathi, C.W. Chu, K.C. Ho, Adv. Mater. 27 (2015) 7229–7235.
[17] J.C. Yu, Y.J. Cui, H. Xu, Y. Yang, Z.Y. Wang, B.L. Chen, G.D. Qian, Nat. Chem. 4 (2013) 2719.
[18] J.P.Q. Jiang, D.W. Feng, H. Cai. Zhou, Angew. Chem. Int. Ed. 55 (2016) 7188–7193.
[19] Y.H. Fu, D.R. Sun, Y.J. Chen, R.K. Huang, Z.X. Ding, X.Z. Fu, Z.h. Li, Angew. Chem. Int. Ed. 51 (2016) 3364–3367.
[20] C. Wang, Z.G. Xie, K.E. DeKrafft, W.B. Lin, J. Am. Chem. Soc. 133 (2011) 13445–13454.
[21] D.K. Wang, R.K. Huang, W.J. Liu, D.R. Sun, Z.H. Li, ACS Catal. 4 (2014) 4254–4260.
[22] K.M. Choi, D. Kim, B. Rungtaweevoranit, Christopher A. Trickett, J.T.D. Barmanbek, A.S. Alshammari, P.D. Yang, O.M. Yaghi, J. Am. Chem. Soc. 139 (2017) 356–362.
[23] L. Ye, J.X. Liu, Y. Gao, C.H. Gong, M. Addicoat, T. Heine, C.W.L.C. Sun, J. Mater. Chem. A 4 (2016) 15320–15326.
[24] H.B. Zhang, J. Wei, J.C. Dong, G.G. Liu, L. Shi, P.F. An, G.X. Zhao, J.T. Kong, X.J. Wang, X.J. Meng, J. Zhang, J.H. Ye, Angew. Chem. Int. Ed. 55 (2016) 14310–14314.
[25] H.Q. Xu, J.H. Hu, D.K. Wang, Z.H. Li, Q. Zhang, Y. Luo, S.H. Yu, H.L. Jiang, J. Am. Chem. Soc. 137 (2015) 13440–13443.
[26] Y.Y. Liu, Y.M. Yang, Q.L. Sun, Z.Y. Wang, B.B. Huang, Y. Dai, X.Y. Qin, X.Y. Zhang, ACS Appl. Mater. Interfaces 5 (2013) 7654–7658.
[27] E.Y. Choi, C.A. Wray, C.H. Hu, W.Y. Choe, CrystEngComm 11 (2009) 553–555.
[28] P.E. Kolic, N. Siraj, S. Hamdan, B.P. Regmi, I.M. Warner, J. Phys. Chem. C 120 (2016) 5155–5163.
[29] M.T. Zhao, Y.X. Wang, Q.L. Ma, Y. Huang, X. Zhang, J.F. Ping, Z.C. Zhang, Q.P. Lu, Y.F. Yu, H. Xu, Y.L. Zhao, H. Zhang, Adv. Mater. 27 (2015) 7372–7378.
[30] X.C. Jiao, Z.W. Chen, X.D. Li, Y.F. Sun, S. Gao, W.S. Yan, C.M. Wang, Q. Zhang, Y. Lin, Y. Luo, Y. Xie, J. Am. Chem. Soc. 139 (2017) 7586–7594.
[31] J.N. Qin, S.B. Wang, X.C. Wang, Appl. Catal. B: Environ. 209 (2017) 476–482.
[32] Y.X. Pan, Y. You, S. Xin, Y.T. Li, G.T. Fu, Z.M. Cui, Y.L. Men, F.F. Cao, S.H. Yu, J.B. Goodenough, J. Am. Chem. Soc. 139 (2017) 4123–4129.
[33] Y.F. Xu, M.Z. Yang, B.X. Chen, X.D. Wang, H.Y. Chen, D.B. Kuang, C.Y. Su, J. Am. Chem. Soc. 139 (2017) 5660–5663.
[34] J.G. Hou, S.Y. Cao, Y.Z. Wu, F. Liang, L. Ye, Z.S. Lin, L.C. Sun, Nano Energy 30 (2016) 59–68.
[35] L. Shi, T. Wang, H.B. Zhang, K. Chang, J.H. Ye, Adv. Funct. Mater. 25 (2015) 5360–5367.
[36] S.C. Lian, M.S. Kodaimati, D.S. Dolzhnikov, R. Calzada, E.A. Weiss, J. Am. Chem. Soc. 139 (2017) 8931–8938.
[37] L. Li, S.Q. Zhang, L.J. Xu, J.Y. Wang, L.X. Shi, Chem. Sci. 5 (2014) 3808.
[38] S. Sato, T. Arai, T. Morikawa, K. Uemura, T.M. Suzuki, H. Tanaka, T. Kajino, J. Am. Chem. Soc. 133 (2011) 15240–15243.
[39] T.M. Suzuki, H. Tanaka, T. Morikawa, M. Iwaki, S. Sato, Chem. Commun. 47 (2011) 8673–8675.
[40] H.W. Huang, J.J. Lin, G.B. Zhu, Y.X. Weng, X.X. Wang, X.Z. Fu, J.L. Long, Angew. Chem. Int. Ed. 55 (2016) 8314–8318.
[41] L. Vincze, F. Sandor, J. Pem, G. Bosnyak, J. Photochem. Photobiol. A: Chem. 120 (1999) 11–14.
[42] T. Ouyang, H.H. Huang, J.W. Wang, D.C. Zhong, T.B. Lu, Angew. Chem. Int. Ed. 56 (2017) 738–743.